ChemPubSoc Europe

DOI: 10.1002/chem.201502866

CHEMISTRY
A European Journal
Full Paper

Micelles

Controlled Nanopores in Thin Films of Nonstoichiometrically Supramolecularly Assembled Graft Copolymers

Suk Man Cho,[a] Giyoung Song,[a] Sun Kak Hwang,[a] Richard Hahnkee Kim,[a] Jinseong Lee,[a] Seunggun Yu,[a] June Huh,[b] Hui Joon Park,*[c] and Cheolmin Park*[a]

Abstract: Herein, nanometer-scale morphologies of graft-copolymer-like supramolecular thin films, composed of sulfonic acid terminated polystyrene (SPS) and poly(2-vinylpyridine) (P2VP), and their application to antireflection coatings were investigated. The intermolecular complexes of SPS and P2VP, formed through nonstoichiometric multiple hydrogen bonding between the sulfonic acid group of SPS and the nitrogen atom in pyridine unit of P2VP, occurring in film deposition allowed for the formation of spherical micelles (with SPS and P2VP as the corona and core, respectively) in the thin film. Interestingly, the domain size of the micelles was tunable from approximately 20 to 90 nm on average by controlling either the blend ratio of components or the concentration of polymer solution. Furthermore, nanoporous thin films could be easily prepared by removing the core of micelle-based nanostructures by using a simple solvent etching process, leaving sulfonic acid groups on the surface of nanopores, which can be utilized as potential functional sites. Those resultant nanoporous thin films were conveniently employed as an antireflection layer on a glass substrate, giving a maximum 97.8% transmittance in the visible wavelength range.

Introduction

The bottom-up approach, based on molecular self-assembly that can utilize molecular-level building blocks for nanometer-scale pattern formation, has been highlighted as a promising candidate for next-generation nanopatterning technology due to the easy and cost-effective accessibility to sub-10 nm scale dimensions.[1–4] Furthermore, even three-dimensionally defined, complex nanostructures can be easily prepared by molecular self-assembly without any expensive additional devices. In particular, self-assembled systems of macromolecules have been of great interest, including biopolymers,[5] reactive blends,[6–9] and block copolymers,[10–14] among which block copolymers have been widely utilized to fabricate tens-of-nanometer-scale nanopatterns during the last few decades. Thermodynamically incompatible polymers of a block copolymer repel each other and undergo microphase segregation due to covalent links between the polymers, giving rise to nanoscale ordered structures. By controlling the ratio of each block and their molecular weights, a variety of spatially periodic two- or three-dimensional nanostructures, such as spheres, cylinders, gyroids, and lamellas, can be achieved.[15]

Meanwhile, it has recently been demonstrated that a blend of block copolymer and small molecules,[16–21] or two components of homopolymer with functional groups, which can be connected by noncovalent bonds, such as hydrogen bonding,[22–26] ionic interactions,[27–30] charge-transfer interactions,[31] coordination complexation,[32] and halogen bonding,[33] can be utilized to form block-copolymer-like supramolecular complexes, resulting in various self-assembled nanostructures. Such supramolecular systems not only take advantage of the fact that a block copolymer has nanometer-scale structure formation, but also has additional merits, such as easy control of domain size and structure by simple blending of two polymers, as well as facile etchability of specific domains by dissociating the supramolecular noncovalent bonds, for instance, by using a selective solvent. Additionally, the remaining functional groups on the surface of porous nanostructures, after removing the specific domain, can be further utilized as potential active sites.[34]

Herein, we demonstrate that graft-copolymer-like supramolecular assembly is also useful for fabricating nanostructured thin films with size-controllable nanopores. Our supramolecular assembly is based on nonstoichiometric hydrogen bonding in film deposition between the hydrogen atom in the acid end group of sulfonic acid terminated polystyrene (SPS) and the nitrogen atom in the pyridine unit of poly(2-vinylpyridine) (P2VP). A thin nanostructured film consisting of closely packed micelles of the graft-copolymer-like complexes with

[a] S. M. Cho, G. Song, S. K. Hwang, R. H. Kim, J. Lee, S. Yu, Prof. C. Park
Department of Materials Science and Engineering
Yonsei University, Seoul, 120-749 (Republic of Korea)
E-mail: cmpark@yonsei.ac.kr

[b] Prof. J. Huh
Department of Chemical and Biological Engineering
Korea University, Seoul, 136-713 (Republic of Korea)

[c] Prof. H. J. Park
Department of Electrical and Computer Engineering
Division of Energy Systems Research
Ajou University, Suwon, 443-749 (Republic of Korea)
E-mail: huijoon@ajou.ac.kr

Supporting information for this article is available on the WWW under http://dx.doi.org/10.1002/chem.201502866.

cores and coronas of P2VP and SPS, respectively, readily formed by spin coating. Beneficially, the micelles varied in size from approximately 20 to 90 nm on average as a function of either the blend ratio of the components or the concentration of polymer solutions. The subsequent mild etching of cores of the micelles by a selective solvent leads to a thin nanoporous film, the pore size and porosity of which can be controlled. Furthermore, the porosity-controlled nanoporous films were successfully applied for as antireflection (AR) coatings, giving rise to a maximum of 97.8% transmittance in the visible wavelength range.

Results and Discussion

Figure 1a shows the supramolecular self-assembly of SPS and P2VP. Through the hydrogen bond between the sulfonic acid group of SPS and the nitrogen atom in the pyridine unit of P2VP, graft-copolymer-like supramolecules, composed of SPS graft and P2VP backbone, can be formed. Because benzene is a relatively poor solvent for the P2VP polymer chains, they tend to reduce the interface area with benzene, whereas the SPS polymer chains, which are compatible, have a much higher interface area with benzene. We expect that these supramolecules can be assembled into micellar structures, which consist of the P2VP core and SPS corona when the film is formed. Supramolecular bonding between the sulfonic acid group of SPS and the nitrogen atom in the pyridine unit of P2VP could be indirectly confirmed by checking the H_2O content of several polymer films: those containing SPS only, P2VP only, PS-*b*-P2VP block copolymer, or a mixture of SPS and P2VP (SPS–P2VP; weight fraction of P2VP $\approx$ 0.4) by using FTIR spectroscopy. All polymer concentrations in solutions were fixed at 1 wt%. Because nitrogen atoms in the pyridine unit of P2VP can react with H_2O molecules in the atmosphere, the appearance of a band at $\lambda \approx 3375$ nm, which corresponds to vibration of the hydroxyl groups of H_2O molecules, indicates that certain pyridine units of P2VP remain unreacted in the films. The suppression of the band intensity of the SPS and P2VP mixture in the thin film (SPS–P2VP) apparently suggests that most functional sites of the pyridine unit are noncovalently connected to a sulfonic acid group of SPS for supramolecular complexes and only a small number of sites remain active for H_2O (Figure 1b).

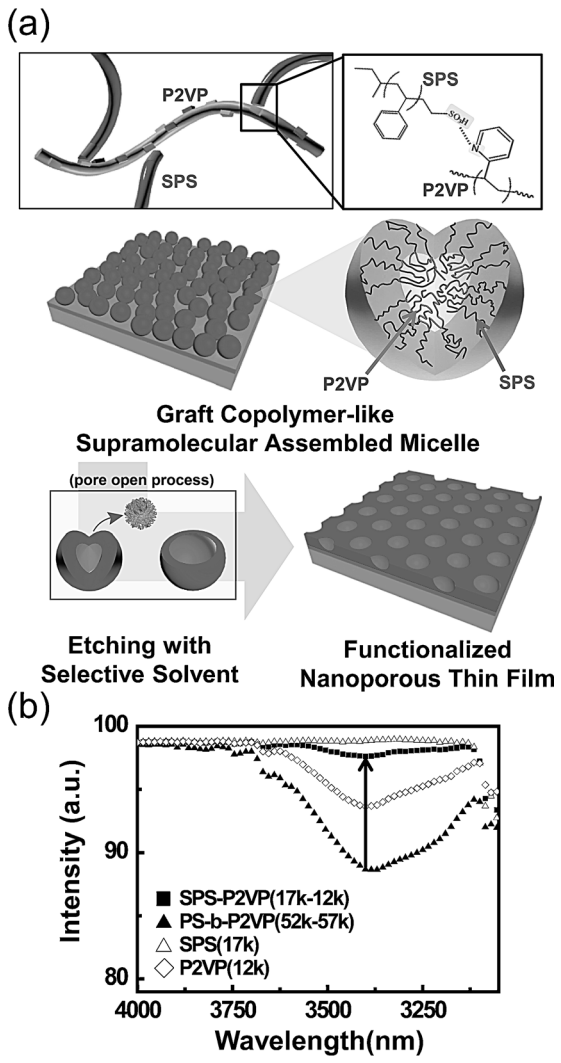

Figure 1. a) Scheme of micelle structure and porous thin film formation through supramolecular interactions. b) FTIR spectra of supramolecular blend film (SPS–P2VP); block copolymer (PS-*b*-P2VP); and homopolymers (SPS and P2VP), which signify hydrogen bonding in reactive blending.

Spin coating of a solution of supramolecular micelles produced a thin polymeric film with closely packed micelles. All thin-film samples were prepared by casting 1 wt% polymer solutions on silicon wafer at 4000 rpm for 60 s, and those films were subsequently dried under ambient conditions for 1 day. The tapping-mode (TM) AFM images in Figure 2a–d show the resultant nanostructured films, and it is clearly shown that nanoscale micellar structures develop in the thin film, even without any surfactant, which is often needed to disperse micelles uniformly. It should be noted that no supramolecular micelles developed in the solution state, as confirmed by dynamic light scattering (DLS) results of the initial solutions and the micelles formed during rapid evaporation of the solvent during spin coating (Figure S1 in the Supporting Information). We further investigated the morphology of a supramolecularly assembled film prepared upon very slow drying. The film shows again closely packed micelles, but their size was much larger than that of micelles obtained during rapid spin coating. The solvent removal speed seems to affect the size of the micelles, rather than their ordering; this has been frequently observed in block copolymer systems (Figure S2 in the Supporting Information).[35] All diameters of micelle nanostructures were calculated by particle analysis of AFM images by using the ImageJ program; the results are summarized in Figure 2e and detailed histograms are given in Figure S3 in the Supporting Information. The diameter of micelles in the thin film increases as the portion of P2VP increases with a narrow size distribution. The distribution, however, becomes broad at $f_{P2VP} = 0.5$.

Meanwhile, different from covalently bonded block- or graft-copolymer-based micelle systems, in which the dimensions of the micelles are rarely tunable without molecular weight changes[36] or swelling by adding a homopolymer,[37] the

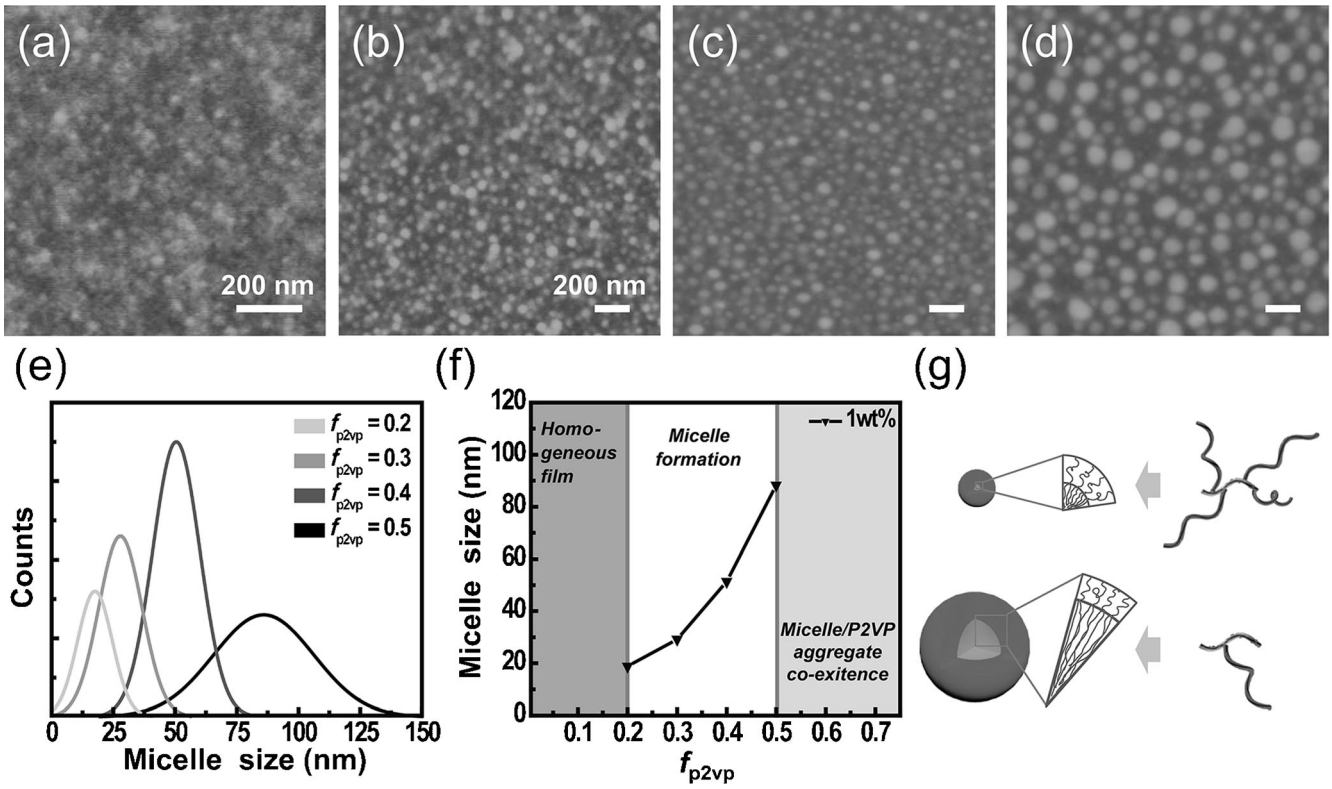

Figure 2. AFM images in height contrast of the supramolecularly assembled SPS–P2VP blend film prepared at different P2VP weight fractions (f_{P2VP}) of 0.2 (a), 0.3 (b), 0.4 (c), and 0.5 (d), with a 1 wt% blend solution. The height scale of each AFM image is a) 5, b) 10, and c)–d) 50 nm. e) Micelle size distributions obtained from the AFM results by particle analysis, and f) the average micelle size values dependent on f_{P2VP}. g) The supramolecular assembly of the graft-copolymer-like blend system allowed for control of micelle sizes by controlling the polymer blend ratio.

domain size of our supramolecular micelles can be readily controlled by the blend ratio of components. The composition of graft-copolymer-like supramolecules, which affects the size of both the core and corona of micelles, can be adjusted according to the blend ratio of SPS and P2VP, as summarized in Figure 2 f. Consequently, by increasing f_{P2VP} from 0.2 to 0.5, the size of the micelle grows from about 20 to 90 nm on average, and even micelles with a maximum diameter of 150 nm were observed for the $f_{P2VP} = 0.5$ sample. Beyond this weight-fraction range, the thin films show miscible blend morphology for $f_{P2VP} < 0.2$, and ill-defined morphologies (a mixture of small micelles and P2VP aggregates coexisting in the structure) were observed for $f_{P2VP} > 0.5$ (Figure S4 in the Supporting Information). The TEM image also confirms the formation of molecules with P2VP cores (Figure S5 in the Supporting Information).

The size variation phenomenon is consistent with the chain number ratio mechanism in a graft copolymer (Figure 2 g). When the micelles form graft copolymers while they were dissolved in good solvent for the corona, it has been found that the more graft chains would make the micelle aggregation numbers low.[38] It can be explained that there are some kinetic limits in corona chains per area of the core. In other words, if the chain ratio increased, the SPS chain number per area in the corona of micelle was not as stable as an identical one with a low chain number ratio because they would be too crowded to be located in the core–shell interface areas, which would make the micelle unstable. Consequently, its size is smaller than that of a graft copolymer system with a low graft chain number ratio. Although there was a report on the supramolecular micelle behavior of P4VP and carboxyl-terminated polybutadiene (CPB) blend in solution, depending on the blend ratio,[39] the authors could not demonstrate micelle nanostructures in the thin-film format for functional nanoporous structures; this is discussed in the next section.

The noncovalent nature of the supramolecular bond offers unique opportunities for functional nanostructures. In our system, the P2VP core, confined within the supramolecular micelle, can be easily removed by a simple solvent etching process. Different from block-copolymer-based systems, the secondary bond between SPS and P2VP, a hydrogen bond in our system, can be easily cleaved and P2VP molecules can be permanently removed by the solvent. For this purpose, the films were immersed in ethanol, a selective solvent for P2VP, to solubilize the P2VP molecules, eventually releasing them from the micelles. It is expected that ethanol molecules selectively penetrate into the P2VP nanodomains, which lowers the density of polymers in P2VP to weaken the hydrogen bonding. Consequently, P2VP molecules can be removed from the micelles to give bowl-like circular nanoporous structures. A similar open core of monolayered micelles upon solvent exposure has been frequently observed in block copolymer systems.[40–42] During core-selective solvent exposure to the micellar thin film, the solvent penetrates through the thin corona and diffuses into the core of the micelle, which makes the core swell. After re-

moval of the solvent, the core that has been swollen shrinks, leaving a void volume, which gives rise to a core-opened micelle film. In our supramolecular case, similar swelling and shrinkage of P2VP cores occurs during solvent treatment, which results in the surface-initiated porous structure.

Meanwhile, the domain sizes of nanopores in all micellar compositions (f_{P2VP} from 0.2 to 0.5), calculated from SEM images (Figure 3a–d), were smaller than those of micelles before etching. The dimension of the micelles, shown in the AFM images (Figure 2), is determined by both P2VP and SPS components, whereas that of the nanopores is defined by only the P2VP core phase, which will be removed by subsequent solvent etching. The domain size of the nanopores, shown in the SEM images (Figure 3), was also calculated by the ImageJ program, similar to that of micelles in the thin film, and their trends are summarized in Figure 3f. Elimination of the P2VP core phase from micelles by a solvent etching process could be further confirmed by XPS (Figure 3g). The strong electron emission peak at 399 eV, which corresponds to the 1s electron peak of nitrogen of the P2VP polymer chains, is significantly suppressed after solvent washing, which means the P2VP nanodomains are removed by ethanol rinsing (Figure 3g). XPS depth profile and FTIR spectroscopy results of an ethanol-etched film further provide evidence for the complete removal of P2VP chains in the film (Figure S6 in the Supporting Information).

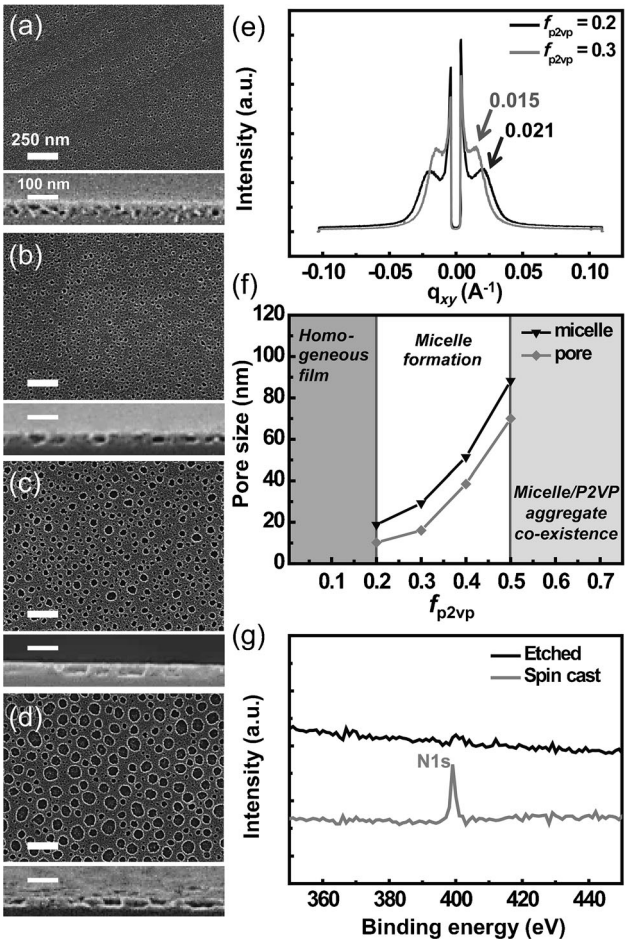

Figure 3. Nanostructures and surface chemical characteristics of SPS–P2VP thin films with different blend ratios after washing with ethanol. The concentration of each polymer solution was fixed at 1 wt%. SEM images of $f_{P2VP} = 0.2$ (a), 0.3 (b), 0.4 (c), and 0.5 (d). e) The 1D grazing-incidence small-angle X-ray scattering (GISAXS) patterns of $f_{P2VP} = 0.2$ and 0.3 blend films. f) Correlation of the average micelle sizes versus f_{P2VP}. g) The X-ray photoelectron spectroscopy (XPS) results for the nitrogen signals of $f_{P2VP} = 0.4$ films before (gray) and after (black) the etching process.

The dimensions of the nanoporous structures were further characterized by GISAXS (Figure 3e). Nanoporous samples with $f_{P2VP} = 0.2$ and 0.3 show the strong first peaks of the in-plane scattering vector, $\mathbf{q}_{xy}$, at 0.021 and 0.015 A^{-1}; this indicates that the domain spacings among the nanopores are approximately 30 and 42 nm, respectively, which are consistent with the results shown in the SEM images. The 2D GISAXS patterns of each film are shown in Figure S7 in the Supporting Information. Unfortunately, scattering signals from the samples with $f_{P2VP} = 0.4$ and 0.5 were not detectable due to their larger dimensions in the films. Another unique property of our supramolecular system is that the sulfonic acid functional groups, which remain on the surface of the SPS nanoporous structure after solvent etching, can be further utilized as potential functional sites for various applications. For example, our former studies, based on an end-functionalized polystyrene and poly(ethylene oxide) polymer blend system, demonstrated that these could be used as the solid-state oxidation and reduction reaction with metallic salt.[34] Meanwhile, solvent vapor treatment could also be utilized for the pore-opening process instead of solvent washing; however, remaining P2VP molecules, which were not permanently removed, induced smaller nanopores (Figure S8 in the Supporting Information). Furthermore, these nanopores could not have functionality on the surface due to the remaining P2VP molecules.

The dimension of our supramolecular micelle was also controllable by changing the concentration of the blend solution. Particle analysis from the SEM (Figure 4a–d) and AFM (Figure S9 in the Supporting Information) images, summarized in Figure 4f, showed that the size of the micelle could increase from about 20 to 80 nm, according to the concentration of solution (from 0.1 to 5 wt%) at a fixed weight fraction of components ($f_{P2VP} = 0.4$). The pore size distributions are shown in Figure S10 in the Supporting Information. Correspondingly, the size of the nanopores in the thin film, prepared by an additional solvent-etching process, could change from about 10 to 75 nm on average, as shown in the SEM images. The dimensions of the nanostructures from both AFM and SEM images were also calculated by ImageJ analysis. This relationship is similar to that of poly(acrylic acid)/polystyrene (PAA-*g*-PS) graft copolymer micelle system in water.[43] The micelle size decreased drastically when the polymer concentration of the solution decreased from about 0.65 to 0.05 wt%. The relationship between concentration and micelle size behavior was controlled by the kinetics of aggregation. Meanwhile, domain spacing among nanopores fabricated from a 0.1 wt% blend solution could be further characterized by GISAXS signals, which showed the strong first peak of in-plane scattering vector, $\mathbf{q}_{xy}$,

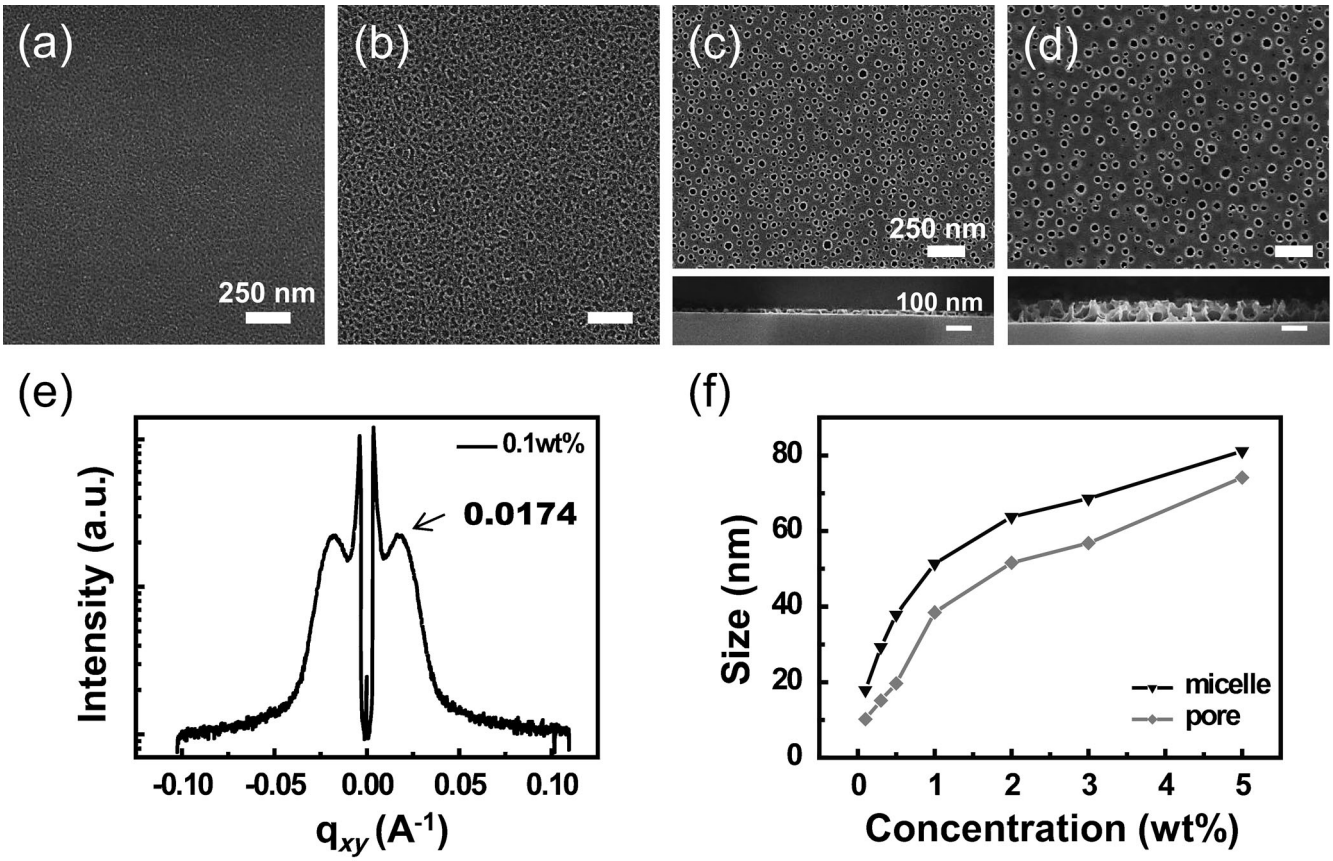

Figure 4. Surface and cross-section views of SEM images of the nanoporous thin films spin cast from 0.1 (a), 0.5 (b), 2 (c), and 5 wt% (d) solutions of SPS–P2VP at a fixed f_{P2VP} of 0.4 and subsequent etching with ethanol. e) The 1D GISAXS pattern of circular nanopores of the 0.1 wt% blend film. f) Changes in micelle and nanopore sizes with different concentrations of polymer solution, as characterized by particle analysis from the AFM image shown in Figure S9 in the Supporting Information and the above SEM results, respectively.

at approximately 0.0174 A^{-1}, which was comparable to a center-to-center distance of 36 nm (Figure 4e); however, other samples could not show strong diffraction signals due to their larger dimensions (Figure S11 in the Supporting Information).

Our nanoporous films with controlled porosity can be utilized for efficient AR coatings (Figure 5). In general, reflection from the film-coated surface is minimized when the refractive index of the coating layer (n_c) is the geometrical mean of the surrounding indices, substrate (n_s) and air (n_{air}), with the equation $n_c=(n_s n_{air})^{1/2}$ approaching about 1.23 on a glass substrate, which has $n_s \approx 1.5$.[44] However, because most single-layered materials have higher values than this, nanoporous films, for which n_c can be adjusted through Equations (1) and (2), which have been widely studied as a promising candidate to approach that value.[45]

$$\text{reflectivity} = \frac{(n_s - n_c^2)^2}{(n_s + n_c^2)^2} \quad (1)$$

$$n_c^2 = n_{polymer}^2(1 - f_{pore}) + n_{air}^2 f_{pore} \quad (2)$$

In Equation (2), $n_{polymer}$ and f_{pore} are the refractive index of the polymer film and the pore volume fraction in the porous film, respectively. In particular, due to the dimensions of the nanopores, which are generated by removing P2VP molecules from the core of the micelle structure by using ethanol etching, being easily changed by adjusting the blend ratio of components and polymer concentration, our system is advantageous to control the refractive index of the nanoporous thin film. Meanwhile, reflection is further minimized by designing the thickness of the AR coating to be one quarter of the wavelength of light in the coating layer ($\lambda/4n_c$), which induces destructive interference between two reflected light waves at the upper and lower boundaries of the AR coating. Therefore, we prepared nanoporous films from 2 wt% solutions, giving thicknesses of about 85 nm to focus on the AR behavior in the visible wavelength. Different sizes of nanopores, according to f_{P2VP} at a fixed solution concentration (2 wt%), are shown in SEM images in Figure S12 in the Supporting Information.

To prepare AR films, a glass substrate was sequentially cleaned by acetone, ethanol, and deionized (DI) water, followed by O_2 plasma treatment for 2 min on both sides. Then, blend films were spin cast on both sides of the substrate. Subsequently, the films were immersed in ethanol to produce the nanoporous structure. Most of resultant AR nanoporous film-coated glasses showed superior transmittances to that of bare glass, and the transmittance was improved with f_{P2VP} (Fig-

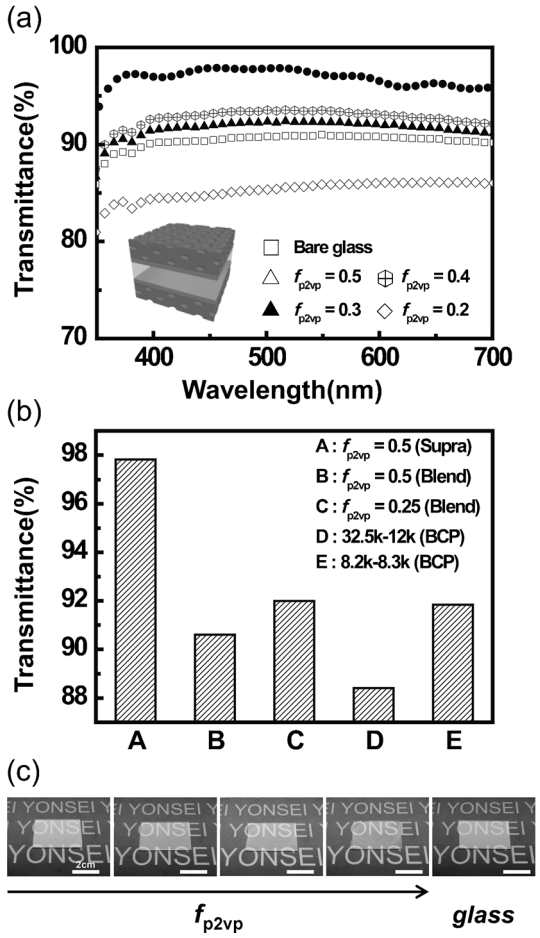

Figure 5. a) Transmittance curves of AR films made from SPS–P2VP blend solutions with different P2VP weight fraction versus wavelength. Inset: a schematic image of the AR sample. b) Transmittance values of AR samples at 500 nm with blended and block copolymer films. c) Photographs of AR samples and bare glass. Each film was made with solutions with different f_{P2VP} values of 0.2, 0.3, 0.4, and 0.5, respectively, with a 2 wt% blend solution.

ure 5a), which affected the portion of nanopores (f_{pore}) according to Equations (1) and (2). The low transmittance of the $f_{P2VP}=0.2$ film may be due to the small portion of nanopores that could not efficiently decrease n_c. Consequently, a maximum transmittance of 97.8% at $\lambda=511$ nm was achieved from the nanoporous film prepared from the $f_{P2VP}=0.5$ blend. The porosity of the films as a function of the weight fraction of P2VP in a supramolecular film was obtained from the reflectance results in Figure 5, and the values are approximately 48.6, 29.8, 25.5, and 2.5% for $f_{P2VP}=0.5$, 0.4, 0.3, and 0.2, respectively. The values are close to those expected for complete removal of P2VP chains. The AR performance depends mainly on the porosity of a film, the refractive index of a substrate, and the refractive index of a porous film matrix. In our system, the optimum porosity for the best AR performance is approximately 69%. Unfortunately, the porous film with 69% porosity was rarely obtained in our supramolecular assembly and the maximum porosity we achieved was 48.6%. The performance we obtained was comparable with those based on block copolymer self-assembly[44] and nanoparticle aggregation.[46]

We also tested AR films of PS-*b*-P2VP diblock copolymers and PS/P2VP homopolymer blends with similar portions of P2VP to a supramolecular assembled nanoporous film with $f_{P2VP}=0.5$ for comparison. The transmittance values at 500 nm of the samples in Figure 5b show the excellent AR performance of our supramolecularly assembled film, which arises from its uniform porous morphology, compared with other samples (Figure S13 in the Supporting Information). To further demonstrate the ability to tune the transmission of a substrate with our nanoporous film, we examined the AR performance of our nanoporous films on sapphire substrates (Figure S14 in the Supporting Information). As expected, the AR performance was tuned as a function of porosity of the films. The best transmittance of approximately 97.7% was also obtained. Our supramolecular films, as shown in Figure 5c, can be an effective way to prepare the efficient nanoporous AR coating for optical devices such as solar cells.

Conclusion

We demonstrated that a supramolecular micelle system could be utilized as a functional nanoporous thin film. For this purpose, polymer blends of end-functionalized SPS and P2VP formed graft-copolymer-like supramolecules through hydrogen bonds. Different from covalently bonded copolymer systems, our supramolecular system has advantages such as the dimension tunability of the nanostructure as well as the easy cleavability of secondary bonds, which are beneficial for generating functional nanostructures with different sizes of nanopores. Furthermore, the functional groups, which remained on the surface of nanotemplates after removing specific domains, could be utilized as potential functional sites. Finally, our supramolecular micelle-based nanoporous thin films showed strong potential as AR films, showing 97.8% transmittance at $\lambda=511$ nm on both glass and sapphire substrates.

Experimental Section

Materials and film preparation

SPS (polydispersity index (PDI)=1.12) and P2VP (PDI=1.08) were purchased from Polymer Source, with molecular weights of 17 and 12 kg mol^{-1}, respectively. Notably, the other end of SPS was a methyl group. The SPS-*b*-P2VP block copolymers were also purchased from Polymer Source with molecular weights of 109, 44.5, and 16.5 kg mol^{-1}, which corresponded to P2VP weight fractions of 0.52, 0.27, and 0.50, respectively. PS with a molecular weight of 35 kg mol^{-1} was purchased from Sigma Aldrich. Benzene and ethanol were purchased from Duksan and Sigma Aldrich, respectively. All chemicals were used as received. One-end-functionalized SPS and P2VP were dissolved in benzene, followed by stirring at 50 °C for 1 day. Subsequent spin coating (SPIN 1200 Midas system, Korea) at a spin rate of 4000 rpm for 60 s produced thin blend films with a thickness of approximately 50 nm (1 wt%) on silicon substrates with a native silicon oxide layer of about 2 nm. The films were dried under ambient conditions for 1 day. The film thicknesses were measured by using an Alpha step 500 surface profiler (AS500). To form the nanoporous structure, the thin films were immersed in ethanol for 20 min.

Antireflection (AR)

The glass substrate was cleaned with acetone, ethanol, and DI water, followed by O_2 plasma treatment for 2 min at 50 V and 40 sccm on both sides. Subsequently, the film was spin cast on both sides of the substrate. The film was dried under ambient conditions for 1 day. Then, the supramolecular and homopolymer blend films were immersed in ethanol for 20 min and the block copolymer films were solvent annealed by ethanol for 1 h. The transmittance of the AR layer-coated glass was detected by UV/Vis spectroscopy (Lambda750, PerkinElmer).

Characterization

TM-AFM (Nanoscope Iva Digital Instruments) was used to characterize the height and phase images of supramolecularly self-assembled thin films. Field-emission scanning electron microscopy (FESEM; JEOL 6701F) in bright-field mode was utilized to characterize the nanoporous films. The GISAXS experiments were conducted at the 9A beam lines of the Pohang Accelerator Laboratory (PAL) in Korea. The operating conditions for GISAXS were set to have a wavelength of 1.2081 Å and a sample-to-detector distance (SDD) of 4 m. The incident angles were changed from 0.09 to 0.19° to probe the surface and internal structures of the entire film by enabling the X-rays to pass through the thin film above the critical angle (α_c) of the thin-film samples. The 2D GISAXS patterns were recorded by using a 2D detector MAR165. TEM (JEM-ARM 200F) was conducted with a beam energy at 80 kV. XPS was measured with a Sigma Probe unit (Thermo VG, UK) at room temperature by using a monochromatic $Al_{K\alpha}$ X-ray source at 15 kV and 300 W. The sample analysis chamber of the XPS instrument was maintained at a pressure of 1.3×10^{-9} mbar. DLS (NanoZS, Malvern) was measured with a quartz cuvette cell because benzene might affect disposable cuvettes composed of PS or poly(methyl methacrylate) (PMMA). A UV/Vis spectrophotometer was operated in transmittance mode from $\lambda = 400$ to 700 nm and the nanoporous film was coated on both sides of the glass substrate. FTIR spectroscopy (Spectrum 100, PerkinElmer) was measured in transmission mode to determine hydrogen bonds in SPS and P2VP.

Acknowledgements

This study was supported by the National Research Foundation of Korea (NRF) grant funded by the Korean government (MEST; no. 2014R1A2A1A01005046) and the Pioneer Research Center Program through the National Research Foundation of Korea funded by the Ministry of Science, ICT and Future Planning (2010-0019313). This research was also supported by the third stage of the Brain Korea 21 Plus Project in 2014 and the X-ray experiments at PAL (9A, beamline), Korea, were supported by MEST and POSCO, Korea.

Keywords: micelles · nanostructures · polymers · supramolecular chemistry · thin films

[1] a) S. Zhang, *Nat. Biotechnol.* **2003**, *21*, 1171 – 1178; b) C. J. Villagómez, T. Sasaki, J. M. Tour, L. Grill, *J. Am. Chem. Soc.* **2010**, *132*, 16848 – 16854; c) R. Yerushalmi, A. Scherz, M. E. van der Boom, *J. Am. Chem. Soc.* **2004**, *126*, 2700 – 2701.

[2] K. Ariga, Y. Yamauchi, G. Rydzek, Q. Ji, Y. Yonamine, K. C. W. Wu, J. P. Hill, *Chem. Lett.* **2014**, *43*, 36 – 68.

[3] W.-P. Lin, S.-J. Liu, T. Gong, Q. Zhao, W. Huang, *Adv. Mater.* **2014**, *26*, 570 – 606.

[4] H. Cabral, K. Kataoka, *J. Controlled Release* **2014**, *190*, 465 – 476.

[5] a) C. Du, G. Falini, S. Fermani, C. Abbott, J. Moradian-Oldak, *Science* **2005**, *307*, 1450 – 1454; b) D. J. Pochan, Z. Chen, H. Cui, K. Hales, K. Qi, K. L. Wooley, *Science* **2004**, *306*, 94 – 97.

[6] C. Koning, M. Van Duin, C. Pagnoulle, R. Jerome, *Prog. Polym. Sci.* **1998**, *23*, 707 – 757.

[7] M. Freluche, I. Iliopoulos, J. J. Flat, A. V. Ruzette, L. Leibler, *Polymer* **2005**, *46*, 6554 – 6562.

[8] H. K. Jeon, J. K. Kim, *Macromolecules* **1998**, *31*, 9273 – 9280.

[9] T. Park, S. C. Zimmerman, *J. Am. Chem. Soc.* **2006**, *128*, 11582 – 11590.

[10] G. Krausch, R. Magerle, *Adv. Mater.* **2002**, *14*, 1579 – 1583.

[11] J. W. Jeong, Y. H. Hur, H.-j. Kim, J. M. Kim, W. I. Park, M. J. Kim, B. J. Kim, Y. S. Jung, *ACS Nano* **2013**, *7*, 6747 – 6757.

[12] T. H. Kim, J. Huh, J. Hwang, H.-C. Kim, S. H. Kim, B.-H. Sohn, C. Park, *Macromolecules* **2009**, *42*, 6688 – 6697.

[13] N. T. Lawrence, J. M. Kehoe, D. B. Hoffman, C. Marks, J. M. Yarbrough, G. M. Atkinson, R. A. Register, M. J. Fasolka, M. L. Trawick, *Macromol. Rapid Commun.* **2010**, *31*, 1003 – 1009.

[14] T. Yamaguchi, H. Yamaguchi, *Adv. Mater.* **2008**, *20*, 1684 – 1689.

[15] a) C. Park, J. Yoon, E. L. Thomas, *Polymer* **2003**, *44*, 6725 – 6760; b) S. B. Darling, *Prog. Polym. Sci.* **2007**, *32*, 1152 – 1204; c) M. Park, C. Harrison, P. M. Chaikin, R. A. Register, D. H. Adamson, *Science* **1997**, *276*, 1401 – 1404; d) H. Cui, Z. Chen, S. Zhong, K. L. Wooley, D. J. Pochan, *Science* **2007**, *317*, 647 – 650.

[16] S.-H. Tung, N. C. Kalarickal, J. W. Mays, T. Xu, *Macromolecules* **2008**, *41*, 6453 – 6462.

[17] B. J. Rancatore, C. E. Mauldin, S.-H. Tung, C. Wang, A. Hexemer, J. Strzalka, J. M. J. Fréchet, T. Xu, *ACS Nano* **2010**, *4*, 2721 – 2729.

[18] J. Kao, P. Bai, V. P. Chuang, Z. Jiang, P. Ercius, T. Xu, *Nano Lett.* **2012**, *12*, 2610 – 2618.

[19] W.-H. Huang, P.-Y. Chen, S.-H. Tung, *Macromolecules* **2012**, *45*, 1562 – 1569.

[20] B. Bharatiya, J.-M. Schumers, E. Poggi, J.-F. Gohy, *Polymer* **2013**, *5*, 679 – 695.

[21] S.-H. Tung, T. Xu, *Macromolecules* **2009**, *42*, 5761 – 5765.

[22] J. Huh, O. Ikkala, G. Ten Brinke, *Macromol. Symp.* **1997**, *121*, 123 – 131.

[23] J. Ruokolainen, R. Mäkinen, M. Torkkeli, T. Mäkelä, R. Serimaa, G. t. Brinke, O. Ikkala, *Science* **1998**, *280*, 557 – 560.

[24] L. M. Pitet, A. H. M. van Loon, E. J. Kramer, C. J. Hawker, E. W. Meijer, *ACS Macro Lett.* **2013**, *2*, 1006 – 1010.

[25] P. Cordier, F. Tournilhac, C. Soulie-Ziakovic, L. Leibler, *Nature* **2008**, *451*, 977 – 980.

[26] C. Tang, E. M. Lennon, G. H. Fredrickson, E. J. Kramer, C. J. Hawker, *Science* **2008**, *322*, 429 – 432.

[27] J. Huh, J. Y. Jung, J. U. Lee, H. Cho, S. Park, C. Park, W. H. Jo, *ACS Nano* **2011**, *5*, 115 – 122.

[28] G. Song, J. E. Kim, S. M. Cho, S. I. Jeon, H. J. Park, J. Huh, C.-H. Ahn, C. Park, *ACS Macro Lett.* **2014**, *3*, 1112 – 1116.

[29] J. Huh, H. J. Park, K. H. Kim, K. H. Kim, C. Park, W. H. Jo, *Adv. Mater.* **2006**, *18*, 624 – 629.

[30] T. P. Russell, R. Jerome, P. Charlier, M. Foucart, *Macromolecules* **1988**, *21*, 1709 – 1717.

[31] C. Wang, Y. Guo, Y. Wang, H. Xu, R. Wang, X. Zhang, *Angew. Chem.* **2009**, *121*, 9124 – 9127.

[32] B. G. G. Lohmeijer, U. S. Schubert, *Angew. Chem. Int. Ed.* **2002**, *41*, 3825 – 3829; *Angew. Chem.* **2002**, *114*, 3980 – 3984.

[33] a) N. Houbenov, R. Milani, M. Poutanen, J. Haataja, V. Dichiarante, J. Sainio, J. Ruokolainen, G. Resnati, P. Metrangolo, O. Ikkala, *Nat. Commun.* **2014**, *5*, 4043; b) P. Metrangolo, F. Meyer, T. Pilati, G. Resnati, G. Terraneo, *Angew. Chem. Int. Ed.* **2008**, *47*, 6114 – 6127; *Angew. Chem.* **2008**, *120*, 6206 – 6220; c) A. Farina, S. V. Meille, M. T. Messina, P. Metrangolo, G. Resnati, G. Vecchio, *Angew. Chem. Int. Ed.* **1999**, *38*, 2433 – 2436; *Angew. Chem.* **1999**, *111*, 2585 – 2588.

[34] G. Song, S. M. Cho, H. J. Jung, R. H. Kim, I. Bae, H. Ahn, D. Y. Ryu, J. Huh, C. Park, *Chem. Eur. J.* **2012**, *18*, 15662 – 15668.

[35] J. N. L. Albert, W.-S. Young, R. L. Lewis, T. D. Bogart, J. R. Smith, T. H. Epps, *ACS Nano* **2012**, *6*, 459 – 466.

[36] Y. Zha, R. Maddikeri, S. Gido, G. Tew, *J. Inorg. Organomet. Polym.* **2013**, *23*, 89 – 94.

[37] A. Urbas, R. Sharp, Y. Fink, E. L. Thomas, M. Xenidou, L. J. Fetters, *Adv. Mater.* **2000**, *12*, 812 – 814.
[38] A. R. Eckert, S. E. Webber, *Macromolecules* **1996**, *29*, 560 – 567.
[39] M. Wang, G. Zhang, D. Chen, M. Jiang, S. Liu, *Macromolecules* **2001**, *34*, 7172 – 7178.
[40] Y. Wang, J. Liu, S. Christiansen, D. H. Kim, U. Gösele, M. Steinhart, *Nano Lett.* **2008**, *8*, 3993 – 3997.
[41] Y. Wang, F. Li, *Adv. Mater.* **2011**, *23*, 2134 – 2148.
[42] N. Kumar, O. Parajuli, J.-i. Hahm, *J. Phys. Chem. B* **2007**, *111*, 4581 – 4587.
[43] Y. Ma, T. Cao, S. E. Webber, *Macromolecules* **1998**, *31*, 1773 – 1778.
[44] S. Walheim, E. Schäffer, J. Mlynek, U. Steiner, *Science* **1999**, *283*, 520 – 522.
[45] W. Joo, H. J. Kim, J. K. Kim, *Langmuir* **2010**, *26*, 5110 – 5114.
[46] K. T. Cook, K. E. Tettey, R. M. Bunch, D. Lee, A. J. Nolte, *ACS Appl. Mater. Interfaces* **2012**, *4*, 6426 – 6431.

Received: July 21, 2015
Published online on ■■ ■■, 0000

FULL PAPER

Hard graft! The graft-copolymer-like supramolecular assembly of end-functionalized polymer and homopolymer blend, based on nonstoichiometric hydrogen bonding, offers size-controllable nanopores. The resultant films were employed as an antireflection layer on a glass substrate, which gave rise to excellent visible-light transmittance (see figure).

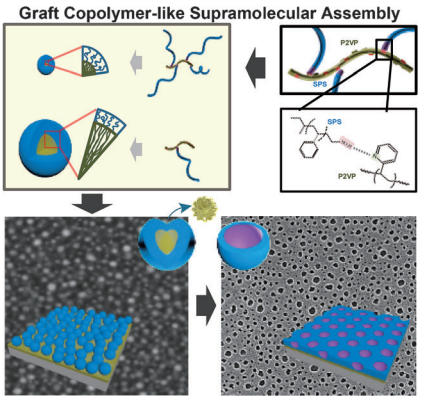

Micelles

S. M. Cho, G. Song, S. K. Hwang, R. H. Kim, J. Lee, S. Yu, J. Huh, H. J. Park, C. Park**

■■ – ■■

Controlled Nanopores in Thin Films of Nonstoichiometrically Supramolecularly Assembled Graft Copolymers